Journal of Materials Chemistry

Cite this: J. Mater. Chem., 2012, 22, 1765

www.rsc.org/materials

COMMUNICATION

Au–Cu alloy bridged synthesis and optoelectronic properties of Au@$CuInSe_2$ core–shell hybrid nanostructures†

Qingfeng Zhang,[a] Jian-jun Wang,[b] Zhiyuan Jiang,*[a] Yu-Guo Guo,[b] Li-Jun Wan,[b] Zhaoxiong Xie[a] and Lansun Zheng[a]

Received 11th October 2011, Accepted 30th November 2011
DOI: 10.1039/c2jm15131f

Based on alloying Cu with Au on the surface of Au nanoparticles (NPs) and using the Au–Cu alloy as a bridge, a multi-step colloid process was successfully developed to prepare Au@$CuInSe_2$ hybrid nanostructures. It has been demonstrated that the as-prepared hybrid nanostructures exhibit excellent optoelectronic properties due to the surface plasmon resonance (SPR) properties of the Au core and the coupling between the Au core and $CuInSe_2$ shell in the Au@$CuInSe_2$ core–shell nanostructure.

In order to improve the overall application performance of nanostructured systems and/or design new functional materials, hybrid nanostructures have attracted increasing research interest.[1–5] On one hand, diverse physical and chemical properties can be integrated into one system. On the other hand, different from the simple mixture of corresponding individual components, the hybrid nanostructures may even show some fascinating properties. Basically, to construct an effective hybrid nanostructure, the properties and functions of the different components should have complementary or synergistic effects. The rational design and synthesis of noble metal–semiconductor hybrid nanostructures is therefore representing a new trend toward advanced functional materials because metallic ingredients can facilitate the charge separation and enhance light absorption in semiconductors, and as a result, improve the photocatalysis and light-harvesting efficiencies of semiconductors.[4–8]

Recently, Au NPs have emerged as an important composite material of hybrid nanostructures because of their metal nature, chemical stability and surface plasmon resonance (SPR) properties.[9–13] On the other hand, I–III–VI_2 semiconductors such as $CuInSe_2$ are one of the most promising light-absorbing materials for photovoltaic applications due to their suitable band gaps, high optical absorption coefficients and good photostability.[14–17] It is reasonable to expect that combining Au and $CuInSe_2$ within a single colloidal nanoparticle may maximize the enhancement of their optical properties and have potentially useful applications. However, as few reports concern the preparation of Au–$CuInSe_2$ hybrid nanostructures,[18] it remains a challenge to develop effective methods to fabricate complicated I–III–VI_2 semiconductors on metal cores. In this communication, based on alloying Cu with Au on the surface of Au NPs and using the Au–Cu alloy as a bridge, a multi-step colloid process was successfully developed to prepare Au@$CuInSe_2$ hybrid nanostructures. It also has been demonstrated that the as-prepared hybrid nanoparticles with core–shell structure exhibit excellent optoelectronic properties, which can be attributed to the enhancement of SPR absorption of the Au core by coupling between the Au core and $CuInSe_2$ shell in the Au@$CuInSe_2$ hybrid nanostructures.

Scheme 1 illustrates the designed scheme for the synthesis of the Au@$CuInSe_2$ hybrid nanostructures through a multi-step injection procedure. Firstly, Au NPs in oleylamine (about 130 °C), Cu(I) and In(III) oleylamine solution (about 130 °C) and Se-oleylamine solution (about 180 °C) were parallelly prepared in three three-neck round bottom flasks connected to a Schlenk line. Secondly, Cu(I) and In(III) oleylamine solution was injected into Au NPs oleylamine solution at 130 °C and the mixture was heated up to 260 °C rapidly for the formation of an Au–Cu alloy layer on the surface of the Au NPs. Thirdly, the Se-oleylamine solution was immediately injected into the above solution for the growth of a $CuInSe_2$ shell on Au NPs.

Fig. 1a is the typical scanning electron microscopy (SEM) image of the products, indicating that a large quantity of nearly spherical particles with the diameter in the range of 60–130 nm were successfully prepared. Fig. 1b is the corresponding transmission electron microscopy (TEM) image. The contrast reveals that these particles have obvious core–shell structures. The diameter of the core is about 30 nm and the shell thickness is in the range of 15–50 nm. The chemical composition of the hybrid nanostructures was investigated by energy-dispersive X-ray (EDX) characterization, which indicates the co-existence of Cu, In, Se and Au (Fig. 1c). The individual TEM image combining the analysis of the cross-sectional compositional line profiles of EDX (Fig. 1d) shows that the core is composed of Au and the shell is composed of Cu, In and Se. The elemental ratio of Cu : In : Se is measured to be 1.00 : 1.05 : 2.14. Considering the error (~5%) of the EDX measurement, the result is in good agreement with

[a]*State Key Laboratory for Physical Chemistry of Solid Surfaces and Department of Chemistry, College of Chemistry and Chemical Engineering, Xiamen University, Xiamen, Fujian, 361005, P. R. China. E-mail: zyjiang@xmu.edu.cn; Fax: +86-592-2183047*
[b]*CAS Key Laboratory of Molecular Nanostructure and Nanotechnology and Beijing National Laboratory for Molecular Sciences, Institute of Chemistry, Chinese Academy of Sciences, Beijing, 100190, P. R. China*

† Electronic supplementary information (ESI) available: Detailed experimental procedures, XPS analysis, HRTEM and SAED of the hybrid nanostructures, UV-vis analysis of Au@$CuInSe_2$ nanostructures, Au NPs and $CuInSe_2$ NPs, and SEM images, TEM images and XRD analysis of the control experiments. See DOI: 10.1039/c2jm15131f

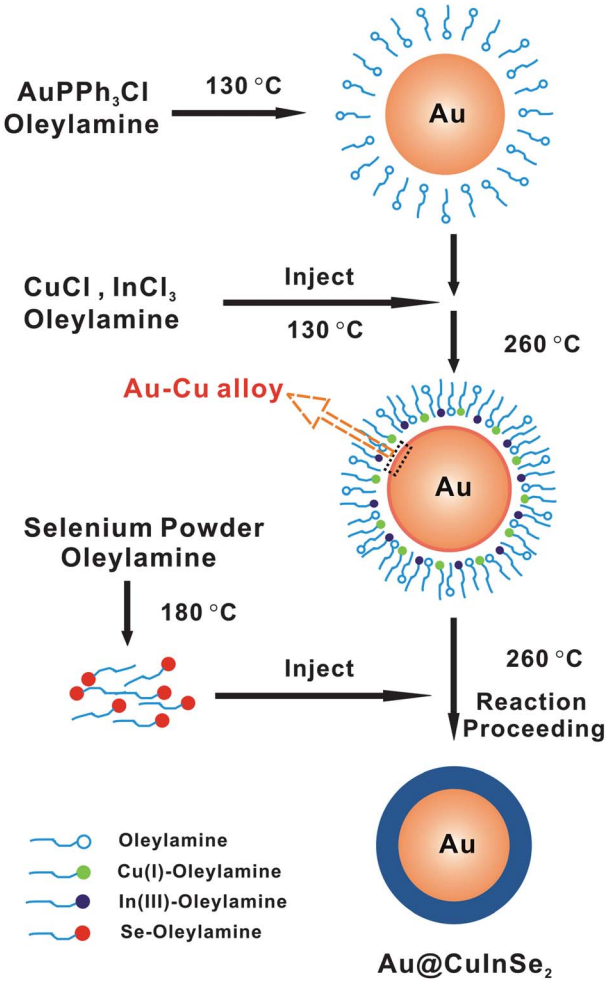

Scheme 1 Schematic illustration of the strategy for synthesis of $Au@CuInSe_2$ hybrid nanostructures through a multi-step injection procedure.

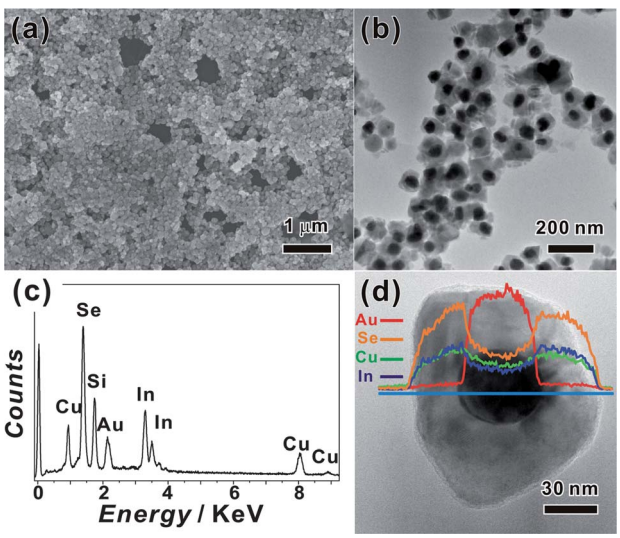

Fig. 1 (a) Typical SEM image, (b) TEM image, (c) EDX spectrum and (d) TEM image combining the cross-sectional compositional line profiles of an individual hybrid nanostructure.

the stoichiometry of $CuInSe_2$. The structure of the as-prepared products could be concluded as $Au@CuInSe_2$ core–shell hybrid nanostructures. The elemental oxidation states of chemical composites of the $Au@CuInSe_2$ were investigated by X-ray photoelectron spectroscopy (XPS) (Fig. S1†), which reveals that the selenium is existed as Se^{2-}, the gold is existed as Au^0, Indium is existed as In^{3+}, and no Cu^{2+} exists in the products. These results also fit with the structure of $Au@CuInSe_2$.[19]

The core–shell nanostructure is one of the most common geometries of the hybrid nanostructures. A lot of methods have been developed to prepare such kinds of core–shell nanostructures. The most widely exploited strategies are based on the "seeded growth" approach. In this scheme, the preformed nanoparticles were referred to as "seed" and served as primary substrate centres for growing shells of different materials. The coating processes, epitaxial growth and oxygen passivation/selective oxidation were three conventional growth mechanisms for the formation of various shells on the metal based cores. The coating processes were widely used to prepare amorphous shells such as SiO_2 and polymer.[20–22] In some cases, the amorphous shell might be further transformed into a polycrystalline shell, *e.g.*, $Au@TiO_2$.[23] The oxygen passivation/selective oxidation process is only suitable for preparing a metal oxide shell.[24–26] Epitaxial growth usually occurs when the core and shell materials are characterized by a similar crystal structure and closely matching lattice parameters.[27–29] In the present case, though the {200} lattice spacing (0.2039 nm) of the face-centered cubic (fcc) Au (JCPDS no.04-0784) crystal is very close to the {220} lattice spacing (0.2046 nm) of chalcopyrite $CuInSe_2$ (JCPDS no. 40-1487) or the {220} lattice spacing (0.2074 nm) of sphalerite $CuInSe_2$ (JCPDS no. 23-0207), the high-resolution TEM (HRTEM) images and selected area electron diffraction (SAED) pattern of a typical $Au@CuInSe_2$ nanostructure show that the shell contains multiple crystal domains and each $CuInSe_2$ nanocrystal adopts different orientations (Fig. S2†). No distinct epitaxial relationship between the Au core and $CuInSe_2$ shell can be found among most of the $Au@CuInSe_2$ nanostructures. Other mechanisms should therefore be included in the growth processing of as-prepared $Au@CuInSe_2$ hybrid nanostructures.

As we know, Cu^+ was easily reduced to Cu^0 in hot oleylamine for the standard reduction potential of Cu^+ is 0.521 V.[30] Furthermore, Cu underpotential deposition (UPD) on the surface of Au substrate may lead to the redox potential of the Au/Cu (UPD) substrate 150 mV more positive than that of Cu^+/Cu^0 (0.521 V).[31,32] It is therefore reasonable to propose that Cu^+ tends to deposit on the Au surface when the hot oleylamine solution contained Cu(I) and In(III) was injected into the Au NPs solution. The newly produced Cu atoms on the surfaces of the Au NPs can easily diffuse into Au NPs and form the Au–Cu alloy layer on the surface of Au NPs.[33,34] Thereafter, the selenization of Cu^0 may be a bridge to grow the $CuInSe_2$ shell on the surface of the Au core. Although the processing is difficult to be *in situ* characterized, the proposed formation mechanism for $Au@CuInSe_2$ nanostructures can be demonstrated by identifying the presence of Au–Cu alloy trace in the X-ray powder diffraction (XRD) patterns of the hybrid nanostructures, as shown in Fig. 2a. The diffraction peaks observed at 26.61, 44.22, 52.40, 64.40, 70.91, 81.38 and 87.54° 2θ can be indexed to the (112), (204)/(220), (312), (400), (316), (424) and (512) of the tetragonal chalcopyrite crystal structure, respectively. The peaks at 38.52, 44.51, 64.64, 77.77 and 82.04° 2θ can be indexed to fcc Au. However, by investigating the XRD patterns carefully, weak shoulder peaks could be found along

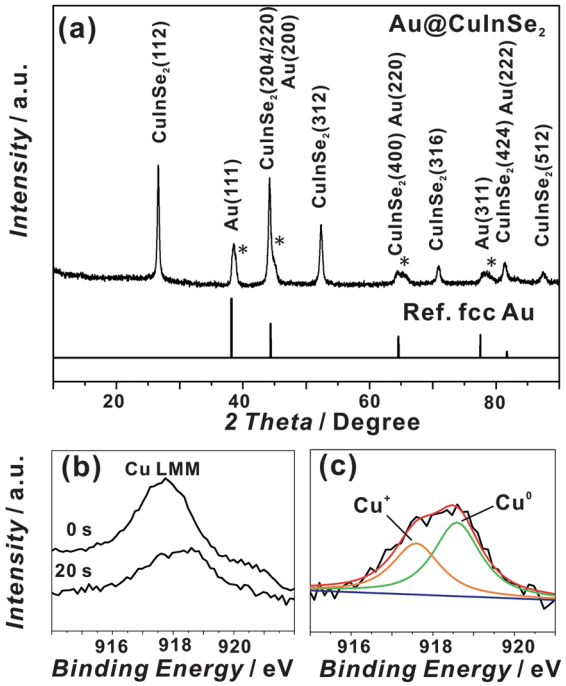

Fig. 2 (a) XRD pattern of $Au@CuInSe_2$ nanocrystals with reference fcc Au (JCPDS no.04-0784) included for comparison. (b) Cu LMM AES spectrum of the surface and at depths of about 20 nm of $Au@CuInSe_2$ nanostructures. (c) The deconvolution result of the Cu LMM AES spectrum at depths of about 20 nm of $Au@CuInSe_2$ nanocrystals.

with the main peaks of fcc Au as marked by stars in the XRD patterns. Those shoulder peaks can be explained by the presence of a thin Au–Cu alloy layer in the present case. The peaks deviating from those of pure Au are caused by the lattice contraction when Cu atoms are alloyed into Au crystal lattice due to that the atomic radii of Cu (0.128 nm) being smaller than that of Au (0.144 nm). Other evidence comes from the Auger Electron Spectroscopy (AES) investigation of the core–shell structures as shown in Fig. 2b. The Cu LMM AES spectrum collected from the surface of the as-prepared core–shell nanostructures shows a characteristic peak at 917.6 eV, matches well with Cu^+ in the $CuInSe_2$ shell. And no signal of Cu^0 was observed, because the Auger electrons collected only come from the surface less than a few nanometres. After the sample was sputtered to about 20 nm depth by an Ar ion gun for 20 s, an asymmetric and broad Auger kinetic energy peak was observed and deconvoluted into two symmetrical peaks centered at around 917.6 and 918.6 eV corresponding to Cu^+ and Cu^0, respectively (Fig. 2c).[19] These results proved the existence of Cu^0 and Au–Cu alloy during the formation of as-prepared hybrid nanostructures.

The proposed mechanism was also confirmed by a series of control experiments. The products prepared by reduction of $AuPPh_3Cl$ in oleylamine at 130 °C were pure Au NPs with a size of about 30 nm (Fig. S3a–c†). When the reaction was quenched at 260 °C without adding the Se source, the Au–Cu alloy layer can form on the surface of the Au NPs (Fig. S3d–f†). And only separated Au NPs and In_2Se_3 flakes can be obtained in the absence of CuCl in the reaction (Fig. S3g–i†). These results proved that the Au–Cu alloy layer on the surface of Au NPs may play a key role in the formation of the $Au@CuInSe_2$ hybrid nanostructures.

It is expected that combining Au and $CuInSe_2$ within a single colloidal nanoparticle may maximize the enhancement of their optical properties. And the hybrid organic–inorganic devices were reported that may take advantage of the easy film-forming properties of organic polymers and the superior properties of inorganic nanoparticles.[35] In order to evaluate the performances of the $Au@CuInSe_2$ core–shell hybrid nanostructures, an organic–inorganic hybrid photodetector combining $Au@CuInSe_2$ core–shell nanostructures with organic poly(3-hexylthiophene) (P3HT) was constructed as illustrated schematically in Fig. 3a.[17,36] The gap width between two electrodes is 35 μm and the length of electrode is 125 μm. The thickness of the hybrid thin film is about 3 μm. As a reference, a similar device combining $CuInSe_2$ nanocrystals with P3HT was also constructed. Typical current–voltage (I–V) characteristics of the photodetectors are shown in Fig. 3b, the hybrid device exhibits high sensitivity to light and the device can also be used as a photoswitch, as shown in Fig. 3c. By switching the light irradiation on and off, the current of the devices shows two distinct states: a "low" current state under dark conditions and a "high" current state under light conditions. The measured response time, defined as the time required for the photocurrent to increase from 10% I_{peak} to 90% I_{peak}, is 0.87 s. The recovery time, which is the time for the photocurrent to decrease

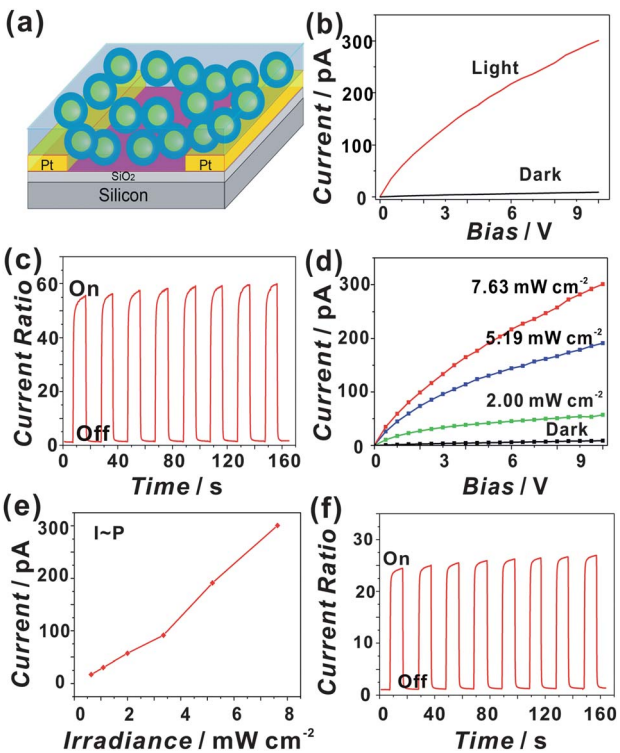

Fig. 3 (a) Schematic illustration of the hybrid device. (b) I–V characteristics of the hybrid device under dark and light conditions. (c) On/off switching of the hybrid device of $Au@CuInSe_2$ nanostructures at an incident density of 7.63 mW cm^{-2} and bias voltage of 1 V. (d) Dark current and photocurrents at different incident light densities of the hybrid device of $Au@CuInSe_2$ nanostructures. (e) Photocurrent measured as a function of incident light density at a bias voltage of 10 V of the hybrid device of $Au@CuInSe_2$ nanostructures. (f) On/off switching of the hybrid device of $CuInSe_2$ nanocrystals at an incident density of 7.63 mW cm^{-2} and bias voltage of 1 V. The current ratio in (c) and (f) was normalized by the dark current.

from 90% I_{peak} to 10% I_{peak}, is 0.45 s (Fig. S4†). Without illumination, the current was only around 1.0 pA. However, at an incident light density of 7.63 mW cm^{-2} and a bias voltage of 1 V, the on/off current ratio was more than 55. The high photoresponse performance of the hybrid devices was further confirmed by photocurrent measurement on the devices at different incident light densities. As shown in Fig. 3d, when the intensity of the incident light was changed, the current of the device changed observably, which could be ascribed to the change of photon density in the incident light at different light intensities. It is well known that the photocurrent response is based on the dissociation of the photogenerated excitons. Thus, the photocurrent shows a strong dependence on the incident light intensity, in accordance with the previous report on photoelectronic devices,[17] and demonstrates a power dependence of ~1.14, that is, $I \approx P^{1.14}$ (Fig. 3e).

For the devices fabricated by combining $CuInSe_2$ nanocrystals with P3HT, the on/off ratio decreased to around 25 under the same conditions (Fig. 3f), which could be caused by the different light absorption ability of the thin film of the devices. The UV-vis spectra of hybrid thin films (Fig. S5†) indicate that the Au@$CuInSe_2$/P3HT hybrid thin film may significantly enhance the light extinction throughout a broad spectral range in contrast to the $CuInSe_2$/P3HT hybrid thin film. As it is well known, the extinction is the sum of absorption and scattering. In order to clarify whether enhanced absorption occurs in Au@$CuInSe_2$ NPs, the amount of absorption in the extinction spectra measured in the ethanol solutions was estimated *via* a reported correction method.[37] The correctional UV-vis spectra of these samples (Fig. S6†) demonstrate that absorption is the dominant factor in the extinction of Au@$CuInSe_2$ nanostructures. And the Au@$CuInSe_2$ nanostructures obviously enhance the absorption in the range of 650–900 nm in comparison to $CuInSe_2$ nanocrystals, Au NPs and the noninteracting mixture of $CuInSe_2$ nanocrystals and Au NPs, which may be due to the increase of SPR absorption of the Au core by coupling between the Au core and $CuInSe_2$ shell in the Au@$CuInSe_2$ core–shell nanostructures.[38]

It should be pointed out that the P3HT plays an important role in the hybrid device due to its easy film-forming property. For the thin film constructed by the pure nanocrystals, the optoelectronic response was very difficult to observe, which could be attributed to the poor quality of the thin film and the complicated interface among the nanocrystals. On the other hand, the interface of the P3HT: Au@$CuInSe_2$ hybrid film may take advantage of the charge dissociation and transportation. It has been reported that the $CuInSe_2$ nanocrystal has a high electron affinity and could act as the photoelectron acceptor, while the P3HT could act as a hole acceptor and electron donor upon photoexcitation.[17,36] When the Au@$CuInSe_2$ NPs were uniformly embedded into the P3HT matrix, the organic–inorganic hybrid thin film would therefore provide pathways for the different carriers to transport separately, which will effectively alleviate charge recombination.

It is also worth noting that the photodetector has outstanding stability. No obvious degradation of the devices was observed after about thirty cycles. These results demonstrate the promising potential of the hybrid device in the area of light detection and signal magnification.

In summary, a multi-step colloid process was successfully developed to prepare Au@$CuInSe_2$ core–shell hybrid nanostructures. Selenium powder was used as the Se source and oleylamine was employed as the surfactant and solvent. The preformed Au NPs were employed as "seeds" and served as primary substrate centres for growing $CuInSe_2$ shells. A mechanism based on an Au–Cu alloy bridge was proposed to explain the formation of a $CuInSe_2$ shell on the Au core. It is anticipated that the strategy demonstrated in the present case may also be applied to synthesize other promising core–shell hybrid nanostructures. It was also demonstrated that the as-prepared hybrid nanostructures exhibit excellent optoelectronic properties and the promising potential of the hybrid device in the area of light detection and signal magnification.

Acknowledgements

We thank Prof. Bin Ren and Mr. Bi-Ju Liu for the help in analysing the UV-vis spectra. This work was supported by the National Natural Science Foundation of China (grant no. 21171141, 21021061 and 21073145), Key Scientific Project of Fujian Province of China (grant no. 2009HZ0002-1), and the National Basic Research Program of China (grant no. 2007CB815303 and 2011CBA00508).

Notes and references

1 L. Y. Wang, H. Y. Park, S. I. Lim, M. J. Schadt, D. Mott, J. Luo, X. Wang and C. J. Zhong, *J. Mater. Chem.*, 2008, **18**, 2629.
2 X. J. Wu and D. S. Xu, *Adv. Mater.*, 2010, **22**, 1516.
3 L. Carbone and P. D. Cozzoli, *Nano Today*, 2010, **5**, 449.
4 R. Costi, A. E. Saunders and U. Banin, *Angew. Chem., Int. Ed.*, 2010, **49**, 4878.
5 A. Vaneski, A. S. Susha, J. Rodríguez-Fernández, M. Berr, F. Jäckel, J. Feldmann and A. L. Rogach, *Adv. Funct. Mater.*, 2011, **21**, 1547.
6 P. K. Sudeep, K. Takechi and P. V. Kamat, *J. Phys. Chem. C*, 2007, **111**, 488.
7 K. K. Haldar and A. Patra, *Chem. Phys. Lett.*, 2008, **462**, 88.
8 T. T. Yang, W. T. Chen, Y. J. Hsu, K. H. Wei, T. Y. Lin and T. W. Lin, *J. Phys. Chem. C*, 2010, **114**, 11414.
9 Y. H. Wei, R. Klajn, A. O. Pinchuk and B. A. Grzybowski, *Small*, 2008, **4**, 1635.
10 J. M. Zhu, Y. H. Shen, A. J. Xie and L. Zhu, *J. Mater. Chem.*, 2009, **19**, 8871.
11 C. H. Kuo, T. E. Hua and M. H. Huang, *J. Am. Chem. Soc.*, 2009, **131**, 17871.
12 Z. H. Sun, Z. Yang, J. H. Zhou, M. H. Yeung, W. H. Ni, H. K. Wu and J. F. Wang, *Angew. Chem., Int. Ed.*, 2009, **48**, 2881.
13 X. F. Wu, H. Y. Song, J. M. Yoon, Y. T. Yu and Y. F. Chen, *Langmuir*, 2009, **25**, 6438.
14 B. Li, Y. Xie, J. X. Huang and Y. T. Qian, *Adv. Mater.*, 1999, **11**, 1456.
15 M. G. Panthani, V. Akhavan, B. Goodfellow, J. P. Schmidtke, L. Dunn, A. Dodabalapur, P. F. Barbara and B. A. Korgel, *J. Am. Chem. Soc.*, 2008, **130**, 16770.
16 Q. J. Guo, S. J. Kim, M. Kar, W. N. Shafarman, R. W. Birkmire, E. A. Stach, R. Agrawal and H. W. Hillhouse, *Nano Lett.*, 2008, **8**, 2982.
17 J. J. Wang, Y. Q. Wang, F. F. Cao, Y. G. Guo and L. J. Wan, *J. Am. Chem. Soc.*, 2010, **132**, 12218.
18 Y. M. Xu and Q. Li, *Nanoscale*, 2011, **3**, 3238.
19 C. D. Wagner, in *Practical Surface Analysis*, ed. D. Briggs and M. P. Seah, John Wiley and Sons, 2nd edn, 1990, vol. 1, pp. 595–634.
20 R. Contreras-Caceres, A. Sanchez-Iglesias, M. Karg, I. Pastoriza-Santos, J. Perez-Juste, J. Pacifico, T. Hellweg, A. Fernandez-Barbero and L. M. Liz-Marzan, *Adv. Mater.*, 2008, **20**, 1666.
21 S. X. Xing, L. H. Tan, M. X. Yang, M. Pan, Y. B. Lv, Q. H. Tang, Y. H. Yang and H. Y. Chen, *J. Mater. Chem.*, 2009, **19**, 3286.
22 S. H. Liu and M. Y. Han, *Chem.–Asian J.*, 2010, **5**, 36.
23 Y. L. Chen, B. L. Zhu, M. Y. Yao, S. R. Wang and S. M. Zhang, *Catal. Commun.*, 2010, **11**, 1003.
24 S. Peng, C. Wang, J. Xie and S. H. Sun, *J. Am. Chem. Soc.*, 2006, **128**, 10676.

25 I. S. Lee, N. Lee, J. Park, B. H. Kim, Y. Yi, T. Kim, T. K. Kim, I. H. Lee, S. R. Paik and T. Hyeon, *J. Am. Chem. Soc.*, 2006, **128**, 10658.
26 K. Yu, Z. C. Wu, Q. R. Zhao, B. X. Li and Y. Xie, *J. Phys. Chem. C*, 2008, **112**, 2244.
27 S. E. Habas, H. Lee, V. Radmilovic, G. A. Somorjai and P. D. Yang, *Nat. Mater.*, 2007, **6**, 692.
28 F. R. Fan, D. Y. Liu, Y. F. Wu, S. Duan, Z. X. Xie, Z. Y. Jiang and Z. Q. Tian, *J. Am. Chem. Soc.*, 2008, **130**, 6949.
29 C. L. Lu, K. S. Prasad, H. L. Wu, J. A. Ho and M. H. Huang, *J. Am. Chem. Soc.*, 2010, **132**, 14546.
30 E. Y. Ye, S. Y. Zhang, S. H. Liu and M. Y. Han, *Chem.–Eur. J.*, 2011, **17**, 3074.
31 E. Herrero, L. J. Buller and H. D. Abruña, *Chem. Rev.*, 2001, **101**, 1897.
32 L. Zhang, J. W. Zhang, Q. Kuang, S. F. Xie, Z. Y. Jiang, Z. X. Xie and L. S. Zheng, *J. Am. Chem. Soc.*, 2011, **133**, 17114.
33 C. L. Bracey, P. R. Ellisb and G. J. Hutchings, *Chem. Soc. Rev.*, 2009, **38**, 2231.
34 W. Chen, R. Yu, L. L. Li, A. N. Wang, Q. Peng and Y. D. Li, *Angew. Chem., Int. Ed.*, 2010, **49**, 2917.
35 W. U. Huynh, J. J. Dittmer and A. P. Alivisatos, *Science*, 2002, **295**, 2425.
36 J. J. Wang, J. S. Hu, Y. G. Guo and L. J. Wan, *J. Mater. Chem.*, 2011, **21**, 17582.
37 N. Micali, F. Mallamace, M. Castriciano, A. Romeo and L. M. Scolaro, *Anal. Chem.*, 2001, **73**, 4958.
38 J. S. Lee, E. V. Shevchenko and D. V. Talapin, *J. Am. Chem. Soc.*, 2008, **130**, 9673.